PEG-grafted chitosan nanoparticles as an injectable carrier for sustained protein release

X. G. Zhang · D. Y. Teng · Z. M. Wu · X. Wang ·
Z. Wang · D. M. Yu · C. X. Li

Abstract The development of injectable nanoparticulate "stealth" carriers for protein delivery is a major challenge. The objective of this work was to investigate the possibility of achieving the controlled release of a model protein, insulin, from PEG-grafted chitosan (PEG-*g*-chitosan) nanoparticles (mean diameter 150–300 nm) prepared by the ion gelation method. Insulin was efficiently incorporated into the nanoparticles, and reached as high as 38%. In vitro release showed that it could control the insulin release by choosing the composition, loading and release temperature. We observed that the composition of the nanoparticle surface (C/O ratio) increased from 2.40 to 3.23, with an increase in the incubation time. Therefore, we concluded that during this time, insulin release from PEG-*g*-chitosan nanoparticles followed a diffusion mechanism in which erosion was negligible. The experiments also demonstrated that PEG-*g*-chitosan helped to maintain the natural structure of the protein entrapped in the nanoparticles.

1 Introduction

In recent years, biodegradable polymeric nanoparticles have attracted considerable attention as potential drug delivery devices, in view of their application in the controlled release of drugs, their ability to target particular organs/tissues, as carriers of DNA in gene therapy, and in their ability to deliver proteins, peptides and genes through an injectable route of administration [1]. With their easy accessibility in the body, nanoparticles can be transported via the circulation to different body sites. Various polymers deliver the drug to a target site and thus increase the therapeutic benefit, while minimizing side effects. Moreover, the hydrophilic nanoparticles generally have longer circulation in blood [2]. Such systems may not only control the rate of drug administration that prolongs the duration of the therapeutic effect, but also deliver the drug to specific sites.

Chitosan is generally recognized as a biocompatible and biodegradable polysaccharide, which exhibits low toxicity [3]. Chitosan nanoparticles have many advantages, such as mild preparation conditions and an excellent capacity for protein entrapment [4]. Moreover, chitosan nanoparticles have proven to be efficient vehicles for the transport of proteins through the mucosa [5, 6]. Although chitosan does possess suitable outstanding properties for various biomedical and pharmaceutical applications, these applications involve blood-contact problems such as hemolysis, thrombosis and embolization, which is due to the fact that chitosan, with a high positive charge, can easily make contact with negatively charged blood corpuscles, which results in hemolysis and toxicity [7, 8].

To overcome these problems, introduction of hydrophilic poly (ethylene glycol) (PEG) and hydrophobic alkyl side chains reduces the adsorption of circulating plasma proteins onto the material surface [7, 9]. As a non-ionic hydrophilic polymer, PEG exhibits outstanding protein resistance, minimal toxicity and immunogenicity. PEG-coated nanoparticles have been found to be of great

X. G. Zhang · D. Y. Teng · X. Wang · Z. Wang · C. X. Li (✉)
Key Laboratory of Functional Polymer Materials, Ministry
Education, and Institute of Polymer Chemistry, Nankai
University, 94 Weijin Road, Tianjin 300071, China
e-mail: lcx@nankai.edu.cn

X. G. Zhang
e-mail: zhangxinge@nankai.edu.cn

Z. M. Wu (✉) · D. M. Yu
Metabolic Diseases Hospital, Tianjin Medical University,
Tianjin 300070, China
e-mail: wuzhongming@tijmu.edu.cn

potential in therapeutic application for controlled release of drugs and site-specific drug delivery [10, 11]. PEG chains that have attached to the surface or formed the corona of a nanoparticle exhibit rapid motion in aqueous media and have a large excluded volume, and steric repulsion results from a loss of configurational entropy of the bound PEG chains [12]. In addition, the hydrophilic PEG can form a hydrated outer shell, which protects the nanoparticles from being quickly uptaken by the reticuloendothelial system [13], extends the half-life of drugs, and alters their tissue distribution.

PEG-modifying chitosan with thermosensitive properties improves blood compatibility of chitosan, and also decreases the enzyme degradation, which is of great interest in therapeutic delivery and tissue engineering [14, 15]. It was found that the potential of PEG-g-chitosan as a safe and more stable gene carrier to the liver [16], and the chitosan–PEG nanocapsules obtained by the solvent displacement technique as new carriers for oral peptide delivery [17]. In addition, PEGylated trimethyl chitosan–insulin nanocomplexes prepared by electrostatic interaction significantly enhanced the uptake of insulin in Caco-2 cells by adsorptive endocytosis [18].

This study aims to develop a chitosan-based injectable, thermosensitive system based upon PEG-g-chitosan that can serve as a therapeutic drug-delivery system through controlled and sustained release of loaded drugs. In this study, insulin was used as a model protein, the interaction between insulin and PEG-g-chitosan and the insulin release behavior of PEG-g-chitosan nanoparticles were studied. Prolonged protein release, which is essential for a number of drug-delivery system applications, was achieved by crosslinking PEG-g-chitosan nanoparticles with sodium tripolyphosphate (TPP) in situ under acid conditions. Also, the effect of polymer composition, drug loading and temperature on the in vitro release of insulin and the release mechanism were investigated.

2 Materials and methods

2.1 Materials

Chitosan (degree of deacetylation 90%, molecular mass 6 and 20 kDa) was obtained from Zhejiang Yuhuan Ocean Biochemical Co., Ltd. (Zhejiang, China). PEG350 (350 Da) and PEG750 (750 Da) were purchased from Aldrich (USA). PEG-g-chitosan (PE3gC64, PE7gC64, PE3gC24 and PE3gC28, with PEG grafting ratio of 26, 29, 26 and 30 wt%, respectively) was prepared as described previously [19]. We used the following abbreviated nomenclature for the copolymers: PEmgCnX, where PEm denotes the molecular mass of PEG in Da, Cn represents the molecular mass of

chitosan, and X shows the molar ratio of PEG/chitosan. The weight of PEG chains grafted per chitosan macromolecule (graft weight ratio) was calculated by elemental analysis.

Pure crystalline porcine insulin (nominal activity 28 IU/mg) that was used without further purification was obtained from Xuzhou Wanbang Biochemical Co., Ltd. (Jiangsu, China). All other chemicals were of analytical grade.

2.2 Preparation of insulin-loaded nanoparticles

For the association of insulin with PEG-g-chitosan nanoparticles, insulin was dissolved in 0.1 M NaOH and then incorporated into 2.0 ml of 1.5 mg/ml TPP solution. The TPP solution was added to 5 ml of 2.5 mg/ml PEG-g-chitosan solution, with stirring at room temperature. Nanoparticles were concentrated by centrifugation at 16,000 rpm for 30 min. Supernatants were discarded and nanoparticles were resuspended in phosphate buffer (pH 7.4) for further in vitro release studies. Process yield of nanoparticles (PY) was calculated as follows:

$$PY = \frac{Particles\ weight}{Total\ solids\ (Polymer\ +\ Insulin\ +\ TPP)\ Weight} \times 100\%$$

2.3 Nanoparticle characterization

Morphological examination of nanoparticles was performed by transmission electron microscopy (TEM) (Philips EM400ST). Samples were placed on copper grids with Formvar films for viewing under the microscope. Particle size was determined by photo-correlation spectroscopy (PCS; BI-200SM).

2.4 Evaluation of insulin-loading capacity of nanoparticles

To determine the association efficiency and PY, triplicate batches of nanoparticles were centrifuged at 16,000 rpm for 30 min at 15°C, and the amount of free insulin in the supernatant was measured by the Bradford method using a UV spectrometer (Shimadzu UV-2550) at 595 nm. The pellet was then lyophilized and weighed. The insulin loading capacity (LC) and the association efficiency (AE) were calculated as follows:

$$AE = \frac{Total\ insulin\ -\ Free\ insulin}{Total\ insulin} \times 100\%$$

$$LC = \frac{Total\ insulin\ -\ Free\ insulin}{Nanoparticles\ weight} \times 100\%$$

All measurements were performed in triplicate and averaged.

2.5 UV-vis and FTIR measurements

The solid-state UV-vis spectra were recorded at $25 \pm 0.1°C$ on a U-3010 spectrophotometer (Hitachi, Japan) for PE3C24, PE3C24 nanoparticles, and insulin-loaded PE3C24 nanoparticles.

Attenuated total reflectance Fourier transform infrared (ATR FT-IR) spectra were collected using a Bio-Rad FTS-6000 FT-IR single beam spectrometer set at a 4 cm^{-1} resolution, equipped with a deuterated triglycine sulfate (DTGS) detector and a 45° face angle Ge crystal. Each spectrum represented 400 jointly added scans whose ratio was calculated against a reference spectrum obtained by recording 400 jointly added scans of an empty ATR cell. FTIR spectra were used as a qualitative reference of protein incorporation into the nanoparticles, and were also used to verify the presence of specific chemical groups in the insulin-loaded PEG-g-chitosan nanoparticles.

2.6 CD-spectroscopy

CD spectra were recorded on a Jasco-715 Spectropolarimeter (JASCO, Tokyo, Japan) at 25°C under a constant flow of nitrogen gas. Typically a cell with a 0.1 cm path length was used for spectra recorded between 190 and 260 nm with sampling points every 0.1 nm. The spectra represent the average of 8–20 scans. CD intensities reported in the figures are expressed in (mdeg).

2.7 Swelling measurements

To understand the effect of the molecular transport of liquids into nanoparticles on the drug release rate, swelling measurements were carried out by immersing freeze-dried nanoparticle samples in phosphate buffer (pH 7.4) at 37°C. Once the weight of the hydrated samples had reached a constant value after 30 min incubation, the samples were taken out and blotted off carefully between tissue papers (without pressing hard) to remove the surface-adhered liquid droplets. The swollen microspheres were then weighed on an electronic microbalance (AE 240; Mettler, Switzerland) to an accuracy of ±0.01 mg. These studies were performed in triplicate for each set of formulated samples, and average values were calculated for data analysis. The percentage of equilibrium water uptake was calculated as follows:

$$\text{Water update}(\%) = \frac{W_S - W}{W} \times 100\%$$

Where Ws is the weight of the swollen nanoparticles, and W is the initial weight of nanoparticles.

2.8 In vitro release studies

Insulin release was determined by incubating nanoparticles at 37°C in 2 ml phosphate buffer (pH 7.4), with horizontal shaking. At predetermined time-points, samples were centrifuged and the supernatant was removed and replaced by fresh buffer. The amount of free insulin was determined by the Bradford method, and a calibration curve was made using non-loaded nanoparticles, to correct for the intrinsic absorption of the polymer. In each experiment, the samples were analyzed in triplicate and the error bars represent the standard deviation.

2.9 X-ray photoelectron spectroscopy (XPS)

XPS characterization of bare or hydrophobin-coated substrates was performed on an XPS apparatus (PHI-5300, PHI) employing a monochromatic Mg Kα radiation source. The survey scan range was 0–1,100 eV, and the electron takeoff angle was fixed at 45°. The energy resolution of the analyzer was 0.8 eV, and the sensitivity was 80–1,600 kcps. The peaks in the elemental core-level spectra were fitted using UNIX on an Apollo Domain series 3,500. All the spectra showed a small shift due to charging, and were therefore calibrated in relation to the C1 s peak of contamination (284.8 eV).

3 Results and discussion

3.1 Characterization of PEG-g-chitosan nanoparticles

In the present study, nanoparticles were prepared by a novel inter-ionic gelation method in aqueous medium (pH 3.9), and particles were obtained spontaneously during the process. Recently polymethacrylic acid/chitosan and TPP/chitosan particles were obtained by this technique, which avoided use of any organic solvents, surfactants and steric stabilizers [20, 21]. Ionic interaction between the positive charge of the amino groups in chitosan and the negative charge of the acid groups of polyacrylic acid/TPP can lead to the formation of inter-ionic polymer complexes [3]. Polyionic hydrogels prepared by ionic gelation have the advantage of creating an ionic environment that favors the stabilization of bioactive agents.

In order to investigate the feasibility of preparing PEG-g-chitosan nanoparticles by ionotropic gelation, we adopted a protocol similar to the one previously established for the creation of chitosan nanoparticles by ionic gelation with TPP [21]. The shape of nanoparticles was examined by TEM. Figure 1 shows insulin-loaded nanoparticles with a compact core surrounded by a fluffy coat of PEG. It is likely that PEG covered the chitosan core to form the shell,
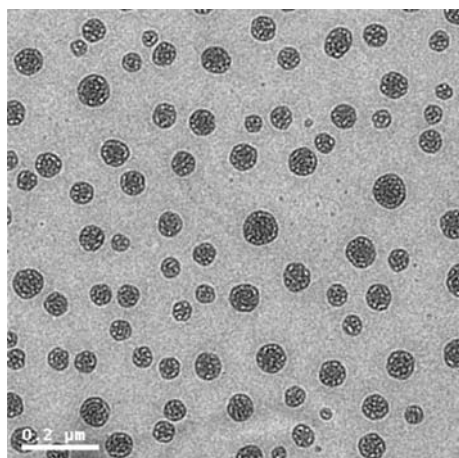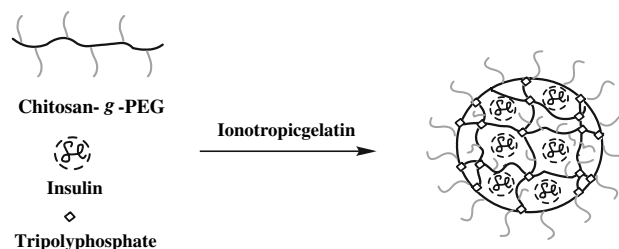
Fig. 1 TEM micrograph of PEG-*g*-chitosan nanoparticles (PEG-*g*-chitosan:TPP, 5:3)

Scheme 1 Schematic illustration of tripolyphosphate-induced micellization behavior of PEG-*g*-chitosan in acid solution

since the PEG end group migrated to the surface of the nanoparticles during the preparation procedure, particularly because of the hydrophilicity of PEG [22]. This was confirmed by the surface charges of nanoparticles: the zeta potential was decreased with an increase in the PEG content from 26 (PE3gC24) to 30 wt% (PE3gC28) (Table 1). This indicates the formation of core-shell nanoparticles (Scheme 1). Calvo et al. have observed that polyethylene oxide (PEO) coats the surface of interpenetrating chitosan/PEO networks nanoparticles prepared by ionic gelation, which has been confirmed by XPS analysis [21].

The particle sizes determined by PCS are shown in Table 1. All nanoparticles prepared by ionotropic gelation were in the size range 160–300 nm. For PE3gC64 and PE7gC64 nanoparticles, increasing the PEG molecular mass from 350 to 750 Da caused the mean particle size to increase from 218 to 286 nm, while increasing the PEG content from 26 to 30 wt% led to an increase of mean particle size from 167 to 175 nm for PE3gC24 and PE3gC28 nanoparticles, respectively. However, Table 1 shows the particle size for PE3gC64 and PE3gC24 decreased from 219 to 167 nm when the chitosan moiety

increased from 6 to 20 kDa. The increase in mean size of the PEG-*g*-chitosan nanoparticles when PEG molecular mass was increased from 350 to 750 Da was expected, and could be attributed to shorter polymer chains giving rise to smaller nanoparticles. However, nanoparticles with the short-chain chitosan, PE3gC64, were unexpectedly larger than those produced from the high-chain chitosan, PE3gC24. Huang et al. have reported that nanoparticles with a short chitosan chain (10 kDa) are unexpectedly larger than those produced from chitosan with a molecular mass of 17–213 kDa, but the mechanism is unclear [23].

The PEG-*g*-chitosan nanoparticles displayed a high loading efficiency (29.1%; Table 1). These results agreed well with the previously reported mechanism of association of protein with chitosan nanoparticles mediated by an ionic interaction between both macromolecules [21]. Scheme 1 illustrates TPP-induced micellization behavior of PEG-*g*-chitosan. Insulin dissolved in NaOH solution is negatively charged (pI 5.3) and consequently, which favors its electrostatic interaction with the positively charged amino groups of chitosan. This mechanism of association was also supported by the observed partial neutralization of nanoparticle surface charge, due to the increasing amount of insulin. In addition, this ionic interaction mechanism may explain the influence of chitosan molecular mass on the insulin LC of the nanoparticles. Indeed, PE3gC24 nanoparticles displayed higher zeta potential values and greater insulin loading efficiencies than PE3gC64 nanoparticles did.

Table 1 The physicochemical properties of PEG-*g*-chitosan nanoparticles

Formulation	PEG (Da)	Chitosan (kDa)	PEG graft (wt%)[a]	The water content (%)	Particle size (nm)[b]	Polydispersity index	Zeta potential (mV)[c]	Loading efficiency(%)[d]	Process yield (%)[e]
PE3gC64	350	6	26	82.1	218.6 ± 2.1	0.11	16.5 ± 0.4	19.5 ± 1.3	58.6 ± 2.2
PE7gC64	750	6	29	76.9	286.5 ± 2.0	0.12	16.6 ± 0.2	23.4 ± 1.9	51.2 ± 3.6
PE3gC24	350	20	26	192.3	166.9 ± 6.6	0.22	29.1 ± 0.3	20.9 ± 2.5	65.4 ± 2.0
PE3gC28	350	20	30	246.1	175.3 ± 2.2	0.24	25.5 ± 1.2	29.1 ± 0.8	57.8 ± 4.1
Chitosan	–	20	–	–	212.4 ± 2.4	0.22	34.5 ± 1.5	12.3 ± 2.6	55.3 ± 3.9

[a] Graft weight % was calculated from the relation: (Wt − Wc)/Wt × 100%, where Wt is the weight of freezed-dried grafted copolymer, and Wc is the weight of chitosan in feed

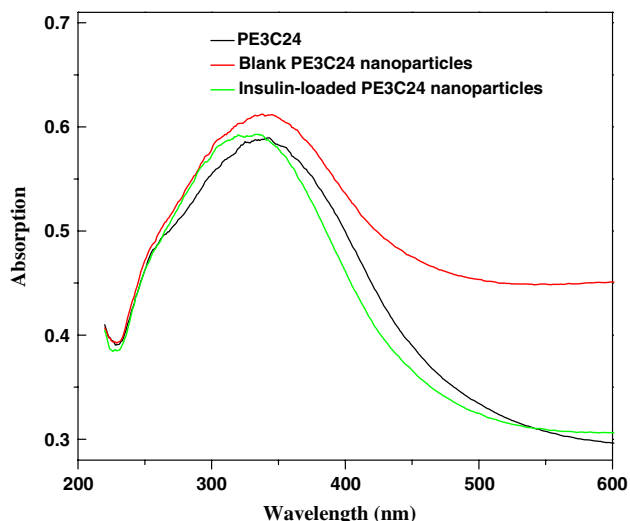[b, c, d, e] Data are given as mean ± sd ($n = 3$)

Fig. 2 UV-vis spectra for PE3C24, blank PE3C24 nanoparticles and insulin-loaded PE3C24 nanoparticles in the solid state

Fig. 3 FT-IR spectra of insulin and insulin-loaded PE3C24 nanoparticles

3.2 UV and IR spectroscopy

The interaction between therapeutic proteins and delivery device may have a significant impact on the efficacy of a recombinant protein-based biological therapy program. To investigate the interaction between insulin and PEG-*g*-chitosan, we monitored the absorption via UV-vis spectroscopy, and conformation via FT-IR spectroscopy.

Figure 2 shows the UV-vis spectra of PE3C24, blank PE3C24 nanoparticles and insulin-loaded PE3C24 nanoparticles in the solid state. The absorption spectrum of PE3C24 displayed a high-intensity $n \rightarrow \pi^*$ band in the UV spectrum (at 343 nm), which corresponded essentially to the absorption of C=O groups of PE3C24. Comparing with the curve for PE3C24, we found that the interaction between TPP and amino groups on chitosan chains did not affect the maximum absorption wavelength, but the band intensity of PE3C24 nanoparticles slightly increased. The absorption spectrum of insulin-loaded PE3C24 nanoparticles had a peak at 328 nm, but the intensity was slightly lower than that of blank nanoparticles. The UV absorption peaks showed a blue shift from 343 to 328 nm in the presence of insulin, which indicated that the interaction between PEG-*g*-chitosan and protein changed the stabilization energy for PEG-*g*-chitosan and TPP [24, 25].

The second-derivative FT-IR spectrum of insulin was dominated by a band of $1,658 \text{ cm}^{-1}$, which indicated a large α-helical content (Fig. 3). β-sheet (1,690 and $1,637 \text{ cm}^{-1}$) and β-turn (1,681 and $1,678 \text{ cm}^{-1}$) contribute little to the secondary structure of insulin in the native state [26, 27]. The insulin amide I (mainly C=O stretching) was observed as a strong bond at $1,658 \text{ cm}^{-1}$, while a band with medium intensity at $1,518 \text{ cm}^{-1}$ of the free insulin was attributed to amide II (C–N stretching and N–H
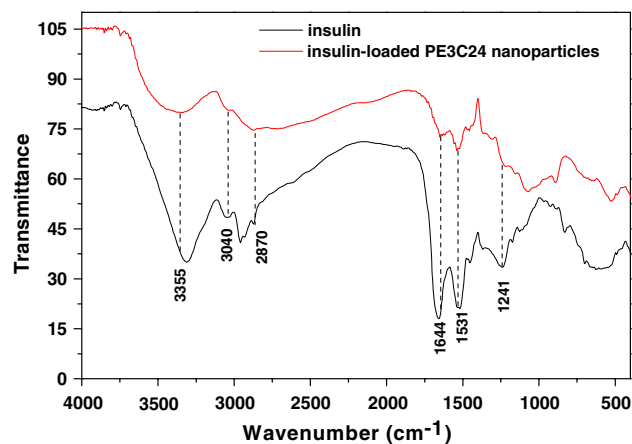
bending modes) vibrations (Fig. 3). FT-IR spectra for insulin were also collected after insulin encapsulation. Figure 3 shows the spectra of insulin entrapped in nanoparticles, collected immediately after production. In comparison with the insulin spectra, a progressive shift of the amide I region towards lower wave numbers (from 1,658 to $1,645 \text{ cm}^{-1}$) was observed in PE3C24 nanoparticles (Fig. 3). The results indicated that the insulin structure was, in general, only slightly affected by association with the nanoparticles. Ionic interactions that occurred between opposite charges of the protein and the polymers may have been responsible for small rearrangements of the protein structure. However, the main peaks corresponding to β-sheet and especially α-helice remained almost unchanged, which indicated that the protein secondary structure was not significantly altered. Sarmento et al. have observed that no significant conformational changes in insulin in alginate/chitosan nanoparticles occur in terms of α-helix and β-sheet content during nanoparticle production [28].

3.3 Circular dichroism spectra

Figure 4 exhibits spectra characteristic of the a-helix structure with two negative peaks at around 223 and 208 nm in the CD spectrum of insulin. The helix content was estimated to be 31.42% from the value of the molar ellipticity at 223 nm in the insulin standard. The addition of PEG-*g*-chitosan affected the circular dichroism band indicating that the helix content of insulin (22.88%) was influenced by the addition of the PE3C24 compound, suggesting that the intermolecular association for this peptide and PEG-*g*-chitosan decreased the content of insulin measured. Pocker and Biswas reported that the helix content depended on the concentration of insulin [29]. Thus, experimental evidence is provided for the fact that
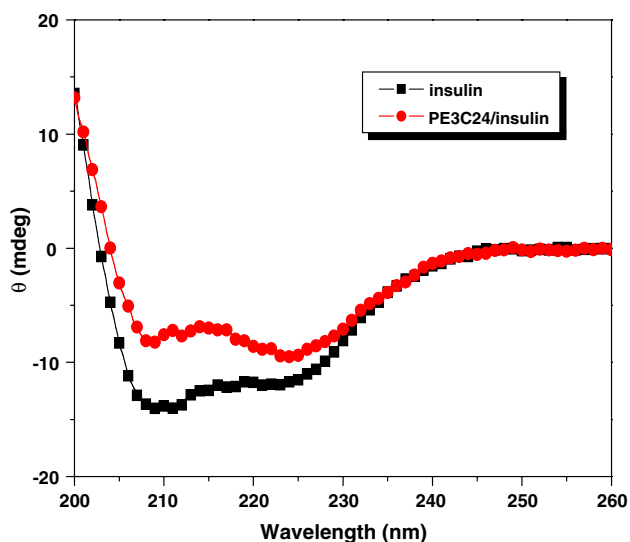
Fig. 4 The CD spectra of aqueous solution of (a) insulin alone, and (b) insulin and PE3C24

Fig. 5 In vitro cumulative release of insulin from PEG-*g*-chitosan nanoparticles: A, PE3gC28; B, PE3gC24; C, PE7gC64; D, PE3gC64; E, Chitosan (2 kDa). Triplicates for each sample were analyzed and each datum point represents the mean ± sd (*n* = 3)

insulin's tertiary structure has not been distorted, so that denaturation cannot be responsible for the inhibitory effect of the polymer.

3.4 Insulin release in vitro

The release of insulin from five types of nanoparticles is displayed in Fig. 5. The overall release process of insulin was biphasic, with an initial burst effect, followed by a levelling-off release phase. The burst effect may have been related to desorption of the protein close to the surface during preparation of the nanoparticles, which then diffused rapidly when the nanoparticles came into contact with the release medium. Later, insulin was released slowly due to swelling or degradation of the polymer. The remaining insulin in nanoparticles was not completely released until the particles were completely eroded or dissolved in release medium, which might have been due to the interaction between the remaining insulin and the few free amine groups on the chitosan segments.

As for copolymer composition, the release rate of insulin mostly depended on chitosan. The release of insulin from PE3gC64 and PE3gC24 nanoparticles was 70% and 16%, respectively, after the first 5 h. The higher molecular mass of chitosan had the longer chain segments and led to an increase in viscosity of the gel layer, which influenced the diffusion of the drug, as well as erosion of the nanoparticles [30]. Portero et al. have observed the great influence of chitosan molecular mass on insulin release from sponges. The lower the chitosan mass, and hence, viscosity, the faster the peptide diffusion through the swollen polymer [31]. As can be observed in Fig. 5, chitosan (2 kDa) nanoparticles presented the slow release
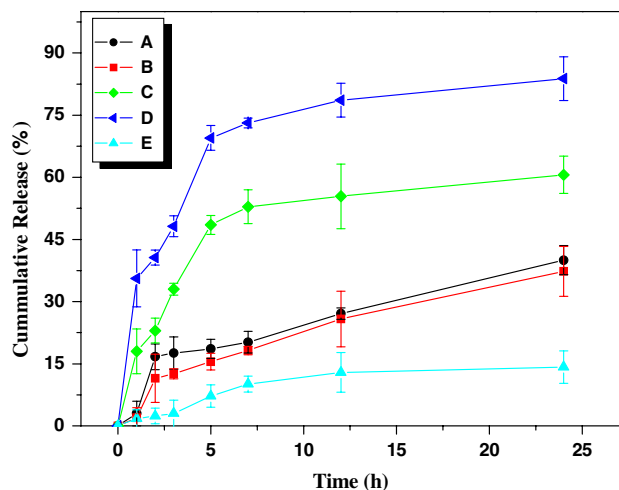
of insulin up to 14% in comparison with that of PE3gC24 (37%) within 24 h, which indicated that the introduction of PEG increased the hydrophilicity of chitosan. Furthermore, the rate of insulin release was affected by the PEG content; as it increased from 26 (PE3gC24) to 30 wt% (PE3gC28), the percentage released increased from 16% to 19% in the first 5 h, which was due to the greater PEG contents and the more hydrophilic nature of the nanoparticles. This was confirmed by the water uptake of nanoparticles (Table 1), which increased with the PEG content of the nanoparticles, which favored drug diffusion. In addition, it can be seen from Fig. 4 that the insulin release profiles from nanoparticles with PEG350 or PEG750 were different, although the chitosan molecular mass was the same (6 kDa). With PEG750, the initial burst was lower (49%) than that from the nanoparticles with PEG350 (70%).

Figure 6 depicts in vitro release of three nanoparticle formulations that contain different amounts of insulin. The results show that released amount depended on the insulin loading in nanoparticles prepared by the same material. As expected, the higher the loading, the more insulin is released. A significant burst was observed from the higher insulin loading nanoparticles (38.2%), which is due to the more insulin absorption on the surface of nanoparticles, leading to a faster release rate in the burst phase. In a levelling-off release phase followed, however, a similar release rate was observed with the variation of loading amount. This indicates the diffusion pathway play an important role in this stage, which led to the decreased concentration gradients (the driving forces for diffusion). Consequently, these results indicate that there were possibilities of modulating the release of insulin for the amount of cumulative release by regulating the loading amount.
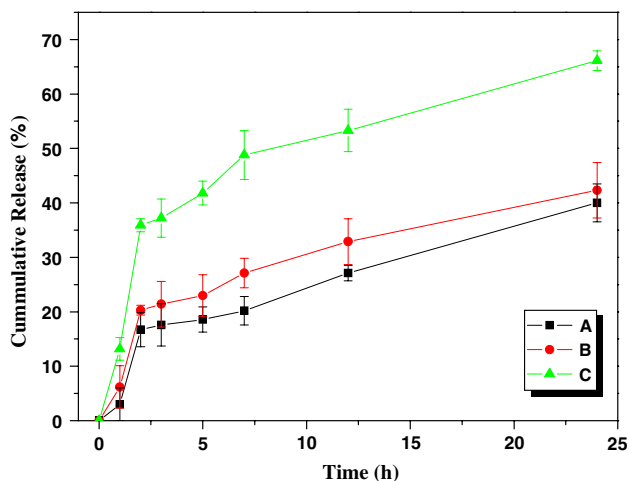
Fig. 6 In vitro cumulative release of insulin from PE3gC28 nanoparticles with different amounts of insulin: A, 29.1%; B, 30.9%; C, 38.2%. Triplicates for each sample were analyzed and each datum point represents the mean ± sd ($n = 3$)

A thermosensitive system based upon PEG-*g*-chitosan hydrogel was developed. This can serve as a therapeutic drug delivery system, which promotes tissue repair and regeneration through controlled and sustained release of loaded drugs. To investigate the effect of temperature on drug release from nanoparticles, we studied the insulin release from PE3gC28 nanoparticles. From Fig. 7, it can be seen that insulin release was up to 89% at 25°C, 81% at 15°C and 40% at 37°C within 24 h, respectively. However, the gelation mechanisms of thermoreversible polymers are quite conceptual and empirical, differing from case to case. No sufficient data is provided for a rigorous explanation of the gelation mechanism involved in the PEG-*g*-chitosan system. However, some indications of molecular
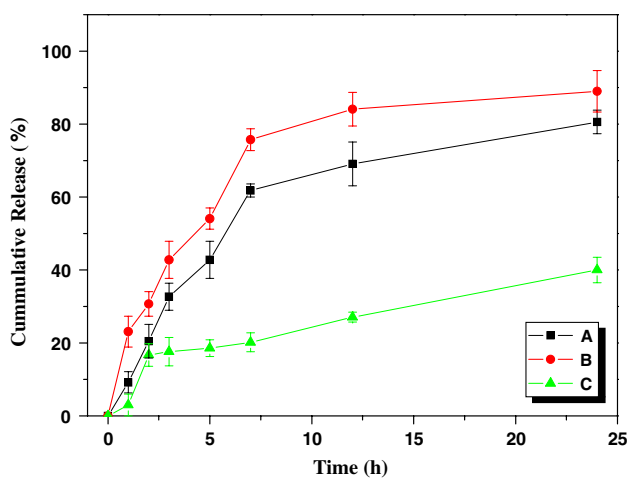

Fig. 7 In vitro cumulative release of insulin from PE3gC28 nanoparticles at different temperature: A, 15°C; B, 25°C; C, 37°C. Triplicates for each sample were analyzed and each datum point represents the mean ± sd ($n = 3$)

interactions might be speculated from the literature published for other thermally sensitive polymer systems [14, 32–34]. The associative forces involved in the PEG-*g*-chitosan system can include hydrophobic interactions between chitosan polymer chains, hydrogen bonding between the OH and NH_2 groups of chitosan, and intermolecular bonding between PEG chains. From a thermodynamic point of view, thermoreversible behavior in a polymer system can generally be regarded as a change of the driving force in response to temperature variation. For PEG-*g*-chitosan system, at low temperatures, chitosan chains are covered with water molecules attached by hydrogen bonds between hydrophilic groups of PEG and water molecules. Thus, the direct association between the polymer chains is disrupted, thereby rendering the graft polymer soluble in water. At 25°C, both chitosan and PEG polymer chains gradually lose the attached water molecules. Moreover, the water mobility increased with the temperature rising, compared with 15°C, which facilitates drug diffusion through the nanoparticles. Increase of testing temperature up to 37°C, however, both chitosan and PEG polymer chains lose the attached water molecules, the interactions between polymer chains start to prevail and a gel forms, which indicates that it is unfavorable for drug diffusion from the nanoparticles. According to the report of Bhattarai et al., chitosan–chitosan hydrophobic interactions play the major role in the thermoreversible gelation behavior of PEG-*g*-chitosan [14].

3.5 Surface analysis

XPS peaks pertaining to C, O and N were scanned at high resolution and deconvoluted to assess the chemical environment of these elements. All samples indicated the presence of C(1 s), O(1 s) and N(1 s) environments (Fig. 8). The C(1 s) peak (284.6 eV) bonded only to C and H, which is attributed to methylene groups. Binding energy C(1 s) located at 286.5 eV is attributed to ether, and that at 288.8 eV to CONH and COOH groups [35]. The O(1 s) spectrum at 532.8 eV is attributed to C–O groups [36]. The N(1 s) peak requires three peaks for the curve fit: at 399.4 eV (amine), 400.5 eV (amide), and 401.4 eV (protonated amine) [37].

It can be seen from Table 2 that low atomic ratios of C/N demonstrated insulin absorbance to the surface of insulin-loaded nanoparticles, compared with blank PEG-*g*-chitosan nanoparticles. As the release time extended (from 0 to 36 h), the ratio of C/N gradually increased from 12.0 to 22.2, while the level of C/O was slightly increased from 2.40 to 3.23 (Table 2). These results show that high density PEG existed on the nanoparticle surface [38]. The high ratios of C/N demonstrated that insulin resorption was

Fig. 8 XPS C1 s, O1 s and N1 s high resolution spectra of PEG-*g*-chitosan nanoparticles at different release time: 0, 8, 18 and 36 h
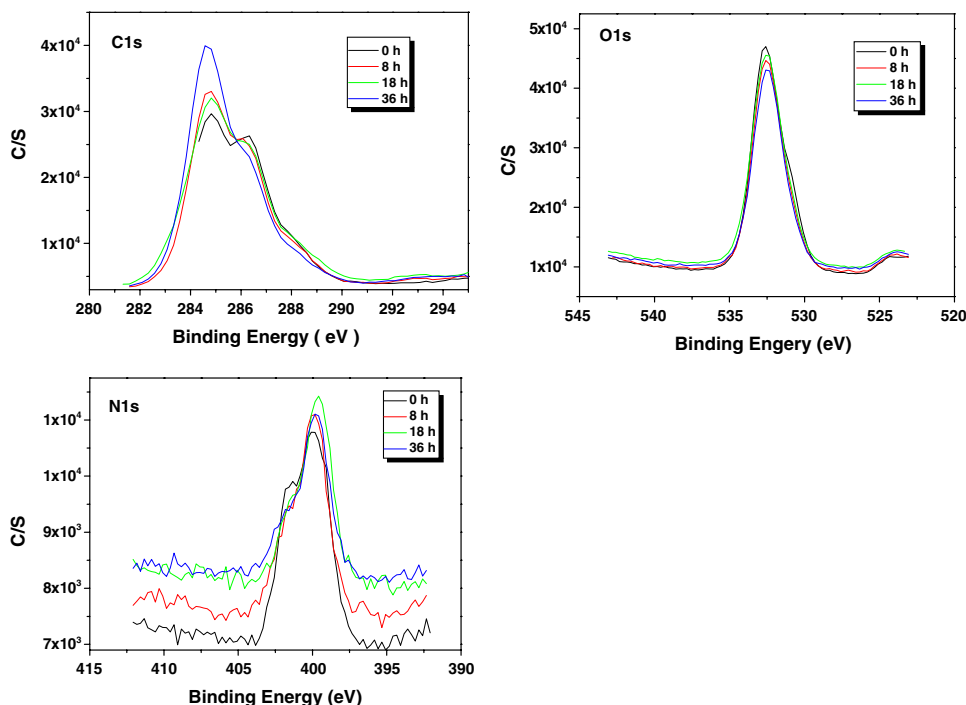

Table 2 Atomic percentage of elements on the surface of insulin-loaded PEG-*g*-chitosan nanoparticles at different release time

Sample	C (%)	O (%)	N (%)	P (%)	C/N	C/O
R0[a]	64.6	26.9	5.4	2.2	12.0	2.40
R8	67.7	24.6	4.3	1.2	15.7	2.75
R16	67.7	24.7	4.0	1.0	16.9	2.74
R36	71.0	22.0	3.2	0.9	22.2	3.23
Blank PEG-*g*-chitosan NPs	65.9	25.9	3.4	2.3	19.4	2.54

[a] Rn stands for the release time of insulin. For example, R0 indicates the release time of insulin is 0 h

counteracted by the steric repulsion of PEG. Furthermore, the high C/O ratio on the nanoparticle surface indirectly indicated that the copolymer was not degraded, which suggests that the mechanism of insulin release is due to diffusion, but not due to polymer degradation. This is similar to the results reported by Bhattarai et al. [14].

4 Conclusion

The nanoparticles were fabricated by chemically grafting monohydroxy PEG on to chitosan chains and TPP. The approach presented in this study had the following favorable attributes: (1) in vitro release of insulin was dependent on the temperature, loading efficiency and composition of the polymer, but its bioactivity was not affected by the interaction between insulin and devices matrix; (2)

nanoparticles have favorable drug release profiles, and after an initial short burst, virtual linear release profiles can be obtained for protein loading studies. Although the present study was targeted at injectable administration, the nanoparticles developed may also have an application in other modes of delivery, such as nasal and oral. Since all the component materials involved have been proven to be tissue-compatible, the nanoparticles are potentially suited for a wide range of in vivo biomedical applications.

References

1. R. Langer, Acc. Chem. Res. **33**, 94 (2000). doi:10.1021/ar9800993
2. E. Allemann, R. Gurny, E. Deolker, Eur. J. Pharm. Biopharm. **39**, 173 (1993)
3. S. Hirano, H. Seino, Y. Akiyama, I. Nonaka, Polym. Eng. Sci. **59**, 897 (1988)
4. K.A. Janes, P. Calvo, M.J. Alonso, Adv. Drug. Deliv. Rev. **47**, 83 (2001). doi:10.1016/S0169-409X(00)00123-X
5. R. Fernández-Urrusuno, P. Calvo, C. Remuñan-Lopez, J.L. Vila-Jato, M.J. Alonso, Pharm. Res. **16**, 1576 (1999). doi:10.1023/A:1018908705446
6. A. Grenha, C.I. Grainger, L.A. Dailey, B. Seijo, G.P. Martin, C. Remuñán-López et al., Eur. J. Pharm. Sci. **31**, 73 (2007). doi:10.1016/j.ejps.2007.02.008
7. M.M. Amiji, Carbohyd. Polym. **32**, 193 (1997). doi:10.1016/S0144-8617(97)00006-4
8. D. Fischer, Y. Li, B. Ahlemeyer, J. Krieglstein, T. Kissel, Biomaterials **24**, 1121 (2003). doi:10.1016/S0142-9612(02)00445-3

9. S. Sagnella, K. Mai-Ngam, Colloids. Surf. B Biointerfaces **42**, 147 (2005). doi:10.1016/j.colsurfb.2004.07.001

10. R. Gerf, Y. Minamitake, M.T. Perracchia, V. Trubetskoy, V. Torchilin, R. Langer, Science **263**, 1600 (1994). doi:10.1126/science.8128245

11. P. Quellec, R. Gref, L. Perrin, E. Dellacherie, F. Sommer, J.M. Verbavatz et al., J. Biomed. Mater. Res. **42**, 45 (1998). doi:10.1002/(SICI)1097-4636(199810)42:1<45::AID-JBM7>3.0.CO;2-O

12. H. Otsuka, Y. Nagasaki, K. Kataoka, Adv. Drug. Deliv. Rev. **55**, 403 (2003). doi:10.1016/S0169-409X(02)00226-0

13. Y. Hu, X.Q. Jiang, Y. Ding, L.Y. Zhang, C.Z. Yang, J.F. Zhang et al., Biomaterials **24**, 2395 (2003). doi:10.1016/S0142-9612(03)00021-8

14. N. Bhattarai, H.R. Ramay, J. Gunn, F.A. Matsen, M.Q. Zhang, J. Control Release **103**, 609 (2005). doi:10.1016/j.jconrel.2004.12.019

15. Y.Q. Hu, H.L. Jiang, C.N. Xu, Y.J. Wang, K.J. Zhu, Carbohyd. Polym. **61**, 472 (2005). doi:10.1016/j.carbpol.2005.06.022

16. X. Jiang, H. Dai, K.W. Leong, S.H. Goh, H.Q. Mao, Y.Y. Yang, J. Gene. Med. **8**, 477 (2006). doi:10.1002/jgm.868

17. C. Prego, D. Torres, E. Fernandez-Megia, R. Novoa-Carballal, E. Quiñoá, M.J. Alonso, J. Control. Release **111**, 299 (2006). doi:10.1016/j.jconrel.2005.12.015

18. S.R. Mao, O. Germershaus, D. Fischer, T. Linn, R. Schnepf, T. Kissel, Pharm. Res. **22**, 2058 (2005). doi:10.1007/s11095-005-8175-y

19. J.M. Harris, E.C. Struck, M.G. Case, M.S. Paley, M. Yalpani, J.M. Van Alstine et al., J. Polym. Sci. Polym. Chem. Ed. **22**, 341 (1984). doi:10.1002/pol.1984.170220207

20. S. Sajeesh, C.P. Sharma, J. Biomed. Mater. Res. B Appl. Biomater. **76**, 298 (2006). doi:10.1002/jbm.b.30372

21. P. LinksCalvo, C. Remuñan-López, J.L. Vila-Jato, M.J. Alonso, Pharm. Res. **14**, 1431 (1997). doi:10.1023/A:1012128907225

22. T. Kaneko, K. Hamada, M.Q. Chen, M. Akashi, Macromolecules **37**, 501 (2004). doi:10.1021/ma035276g

23. M. Huang, E. Khor, L.Y. Lim, Pharm. Res. **21**, 344 (2004). doi:10.1023/B:PHAM.0000016249.52831.a5

24. F. Kong, C.G. Ou, Y. Zheng, S.Y. Zhang, C.Z. Yang, X.L. Wu et al., J. Appl. Polym. Sci. **99**, 2477 (2006). doi:10.1002/app.22842

25. Q.H. Li, T. Yamashita, K. Horie, H. Yoshimoto, T. Miwa, Y. Maekawa, J. Polym. Sci. A Polym. Chem. **36**, 1329 (1998). doi:10.1002/(SICI)1099-0518(199806)36:8<1329::AID-POLA16>3.0.CO;2-8

26. L. Nielsen, S. Frokjaer, J. Carpenter, J. Brange, J. Pharm. Sci. **90**, 29 (2001). doi:10.1002/1520-6017(200101)90:1<29::AID-JPS4>3.0.CO;2-4

27. L. Jøgensen, C. Vermehren, S. Bjerregaard, S. Froekjaer, Int. J. Pharm. **254**, 7 (2003). doi:10.1016/S0378-5173(02)00668-3

28. B. Sarmento, D.C. Ferreira, L. Jorgensen, M. van de Weert, Eur. J. Pharm. Biopharm. **65**, 10 (2007). doi:10.1016/j.ejpb.2006.09.005

29. Y. Pocker, B. Subhasis, Biswas Biochem. **19**, 5043 (1980). doi:10.1021/bi00563a017

30. V.R. Sinha, A.K. Singla, S. Wadhawan, R. Kaushik, R. Kumria, K. Bansal et al., Int. J. Pharm. **274**, 1 (2004). doi:10.1016/j.ijpharm.2003.12.026

31. A. Portero, D. Teijeiro-Osorio, M.J. Alonso, C. Remuñán-López, Carbohyd. Polym. **68**, 617 (2007). doi:10.1016/j.carbpol.2006.07.028

32. S.Q. Liu, Y.Y. Yang, X.M. Liu, Y.W. Tong, Biomacromolecules **4**, 1784 (2003). doi:10.1021/bm034189t

33. B. Jeong, S.W. Kim, Y.H. Bae, Adv. Drug. Deliv. Rev. **54**, 37 (2002). doi:10.1016/S0169-409X(01)00242-3

34. A. Chenite, C. Chaput, D. Wang, C. Combes, M.D. Buschmann, C.D. Hoemann et al., Biomaterials **21**, 2155 (2000). doi:10.1016/S0142-9612(00)00116-2

35. F. Rosso, A. Barbarisi, M. Barbarisi, A. Giordano, J. Mater. Sci. Mater. Med. **15**, 679 (2004)

36. G. Beamson, B.T. Pickup, W. Li, S.M. Mai, J. Phys. Chem. B **104**, 2656 (2000). doi:10.1021/jp9905629

37. G. Lawrie, I. Keen, B. Drew, A. Chandler-Temple, L. Rintoul, P. Fredericks et al., Biomacromolecules **8**, 2533 (2007). doi:10.1021/bm070014y

38. L.Y. Li, S.F. Chen, J. Zheng, B.D. Ratner, S.Y. Jiang, J. Phys. Chem. B **109**, 2934 (2005). doi:10.1021/jp0473321